Clinical Neurophysiology 130 (2019) 2105–2113

Contents lists available at ScienceDirect

Clinical Neurophysiology

journal homepage: www.elsevier.com/locate/clinph

Analysis of electrooculography signals for the detection of Myasthenia Gravis

Timothy Liang [a,1], Mark I. Boulos [b,1], Brian J. Murray [b], Sridhar Krishnan [a], Hans Katzberg [c], Karthikeyan Umapathy [a,*]

[a] Ryerson University, Toronto, ON, Canada
[b] Hurvitz Brain Sciences Research Program, Sunnybrook Research Institute, Sunnybrook Health Sciences Centre, University of Toronto, Toronto, ON, Canada; Department of Medicine, Division of Neurology, University of Toronto, Toronto, ON, Canada; Sleep Laboratory, Sunnybrook Health Sciences Centre, Toronto, ON, Canada
[c] Prosserman Centre for Neuromuscular Diseases, University Health Network/Toronto General Hospital, Toronto, ON, Canada; Division of Neurology, University of Toronto, Toronto, ON, Canada

ARTICLE INFO

Article history:
Accepted 12 August 2019
Available online 23 August 2019

Keywords:
Electrooculogram
Myasthenia Gravis
Sleep test
Time domain analysis
Wavelet domain analysis
Pattern classification

HIGHLIGHTS

- A non-invasive tool for early stage Myasthenia Gravis (MG) screening.
- Quantification of eye movement characteristics elucidating ocular muscle impact of MG disorder.
- Wavelet analysis for detection of eye movement signal morphology relevant for MG classification.

ABSTRACT

Objective: A precursor to more severe forms of Myasthenia Gravis (MG) is ocular MG (OMG) in which the MG symptoms are localized to the eyes. Current MG diagnostic methods are often invasive, painful, and not always specific. The objective of the proposed work was to extract quantifiable features from electrooculography (EOG) signals recorded around the eyes and develop an alternative non-invasive screening method for detecting MG.
Methods: EOG signals acquired from MG and Control subjects were analyzed for eye movement characteristics and quantified using time and wavelet domain signal processing techniques. The ability of the proposed approaches to classify MG vs. control subjects was evaluated using a linear discriminant analysis (LDA) based classifier.
Results: The range of overall classification accuracies achieved by the proposed time and wavelet domain approaches for different groupings were between 82.1–83.3% (Rise Rate feature: $P < 0.01$, AUC ≥ 0.87) and 82.1–87.2% (Mean Scale Band Energy feature: $P < 0.01$, AUC ≥ 0.89), respectively.
Conclusion: Our results demonstrate that an EOG-based signal analysis is a potentially viable non-invasive alternative for MG screening.
Significance: The proposed approach could lead to early detection of MG and thereby improve clinical outcomes in this population.

1. Introduction

Myasthenia Gravis (MG) is a neuromuscular disorder that induces fatigable ptosis or weakness of the extraocular muscles (Kupersmith, 2009). When MG remains localized to the eyes for a prolonged period (>2 years), it is referred to as Ocular Myasthenia Gravis (OMG). 50–80% of patients with ocular symptoms at onset, progress to generalized MG (GMG) (Nair et al., 2014; Gilhus, 2009). Early detection of MG influences treatment plans such as immunotherapy and thymectomy, which can reduce the progression of early MG into more serious forms of GMG (Mee et al., 2003; Sonett et al., 2017). Hence, early detection of MG is vital.

The current electrophysiological methods to diagnose MG are single-fiber electromyography (SFEMG) and repetitive nerve stimulation (RNS). These two approaches have their respective benefits

* Corresponding author at: Dept. of Electrical, Computer, and Biomedical Eng., Ryerson University, Toronto, Canada. Fax: +1 416 979 5280.
E-mail address: karthi@ee.ryerson.ca (K. Umapathy).
[1] First authorship is shared by the two authors.

https://doi.org/10.1016/j.clinph.2019.08.008
1388-2457/

and drawbacks. The advantage of using SFEMG is that it is highly sensitive to detecting abnormalities in neuromuscular transmission (Nair et al., 2014). However, the shortfall of this diagnostic technique is that it is relatively inaccessible as it needs a physician with special training and is not specific for neuromuscular junction defects, as it also is abnormal in neurogenic or myopathic processes. It also causes discomfort to patients due to its invasive nature. The second method, RNS, uses surface electrodes to transmit pulses that induce muscle contraction to detect NMJ fatigability. In comparison to SFEMG, RNS is less invasive and provides higher specificity. Despite RNS being the more common method for initial examinations, SFEMG has higher sensitivity. Apart from RNS and SFEMG, other electrophysiological techniques reported in the literature for detection of MG include use of electrooculography, search coils, infrared, and ocular vestibular evoked myogenic potentials (oVEMP) (Barton, 1998; Azri et al., 2014; Valko et al., 2016), although none of these methods are routinely used clinically in the assessment or diagnostic algorithms of patients with MG or suspected MG.

Early detection of MG via a non-invasive screening method would greatly benefit this clinical population as well as assist treating clinicians. In MG, the eye muscles are often initially affected which is reflected as changes in eye movements that can be non-invasively examined using electrooculography (EOG) signals. EOG signals are routinely collected during in-laboratory sleep studies and there is evidence that MG patients exhibit increased daytime sleepiness and disturbed sleep (Kassardjian et al., 2015; Martínez-Lapiscina et al., 2012). For this study, we used the EOG data collected from MG and Control subjects during two in-laboratory sleep tests, namely the Multiple Sleep Latency Test (MSLT) (Littner et al., 2005) and overnight polysomnography (PSG) (Kushida et al., 2005). Our previous initial study, which used a smaller database size, produced encouraging results when using the number of horizontal slow eye movements extracted from EOG for MG detection (Liang et al., 2016). In this study, we increased the number of control subjects and used advanced signal analyses to ascertain discriminative EOG signal morphologies that could differentiate MG from controls.

2. Methods

2.1. Database

This study was approved by the Sunnybrook Research Ethics Board and written consent was obtained from all patients. The EOG signals were acquired at the Sunnybrook Health Sciences Centre Sleep Laboratory from 8 patients with mild to moderate MG diagnosed by a neuromuscular neurologist, and 31 age- and gender-matched patients, determined by a study neurologist to be free of MG, who served as controls. All signals were sampled at 256 Hz. For each individual patient, we included EOG signals collected during the wake stage of the MSLT and PSG. Using this data, we constructed 3 data sets: (1) Group All – 62 control and 16 MG samples (i.e. data collected from both MSLT and PSG), (2) Group MSLT – 31 controls and 8 MG samples (i.e. data from only the MSLT), and (3) Group PSG – 31 control and 8 MG samples (i.e. data from only the PSG). We examined whether the proposed methods were able to distinguish MG from controls when analyzing MSLT participants alone, PSG participants alone, as well as the combined MSLT and PSG participants. Although the MSLT and PSG data were derived from the same patient, the EOG signals were not identical because the tests were recorded at different times and under different conditions. Moreover, as the generated eye movements were unique and time-varying by nature, the MSLT and PSG signals recorded from the same patient at different times were treated as independent samples. We used a standard EOG acquisition setup (Iber et al., 2007) as is recommended by the American Academy of Sleep Medicine during both MSLT and PSG tests, and provided environments that were conducive to sleep for both tests. Fig. 1 illustrates the electrode placements for the EOG measurement setup i.e., one electrode placed 1 cm below the left outer canthus (LOC) with the signal measured with reference to A2; another electrode placed 1 cm above the right outer canthus (ROC) with the signal measured with reference to A1. These LOC and ROC channel outputs reflected left and right eye movements respectively. A1 and A2 are distant reference electrodes located at the mastoids retroauricularly.

2.2. Pre-processing

During each of the sleep tests, up to 7 h of data were recorded. Based on a previous study (Boulos et al., 2011) and for computational efficiency, we analyzed only the first 10 min of each recorded signal. These 10-min EOG signals [with left (LOC) and right (ROC) channels (Iber et al., 2007)] were then further divided into 30 seconds segments (consistent with the 30-second duration of an epoch in a standard sleep study hypnogram) for more efficient processing.

Since MG induces muscle fatigue, we focused on slow eye movements. In one study (Magosso et al., 2007), most of the slow eye movements were horizontal and fell in the 0.1–1 Hz frequency range. Although various frequencies were observed in the given data, we balanced baseline artifacts against information preservation and used a band-pass filter with a 0.2–1.75 Hz cut-off.

We used both time-domain and wavelet analyses (time-scale) in quantifying discriminative clues that could differentiate MG from control subjects. While our time-domain analysis focused on MG detection, our wavelet analysis focused on capturing characteristic time-scale EOG signal morphologies that could be associated with eye movements in OMG subjects. A future goal of our wavelet analysis is to understand the underlying electrophysiological substrate(s) of the unique EOG signal morphologies that may differentiate MG from control subjects.

2.3. Time domain analysis: eye movement detection algorithm

An eye movement detection algorithm was developed which consisted of 3 main stages: normalization, peak detection, and pulse edge detection. The stages of eye movement detection algorithm are summarized below:

- Stage I: Normalization

$$\tilde{x}[n] = \frac{x[n]}{max|x[n]|} \tag{1}$$

- Stage II: Peak Detection

$$|\tilde{x}[l_i]| \geq 0.25 \cdot max|\tilde{x}[n]| \tag{2}$$

- Stage III: Pulse Edge Detection

$$|x[e(k)]| \geq 0.01 \cdot max|\tilde{x}[n]|, \tag{3}$$

$$e = \begin{cases} 1, \cdots, l_i & \text{if rising edge} \\ l_i, \cdots, M & \text{if falling edge} \end{cases}$$

During the first stage of the eye movement detection algorithm, all segmented signals were amplitude normalized with respect to their segmented portion. Given a segmented signal $x[n]$, the normalization process can be expressed as in Eq. (1). Thresholds

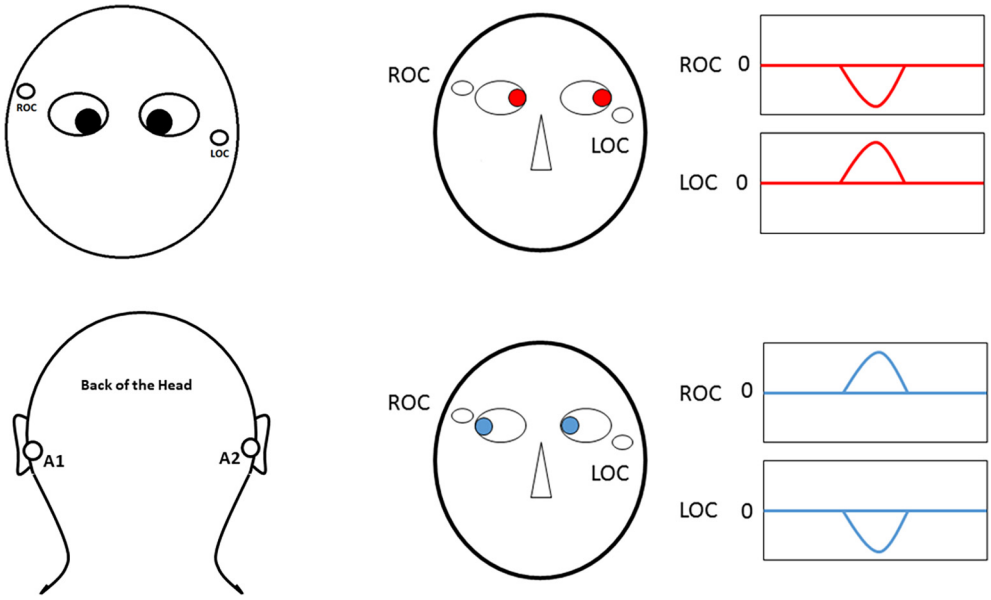

Fig. 1. Electrooculography measurement setup and illustration of Left Outer Canthus (LOC) and Right Outer Canthus (ROC) channels for left and right eye movements.

applied in the algorithm were all relative in nature to avoid the use of absolute measures, which would normally vary among different patient cohorts and measurement settings. Precaution was exercised throughout the study to alienate outliers (identified by visual inspection) that could influence the amplitude normalization process. The peak detection stage identified peaks that occurred in the signal. For the peak detection stage of the algorithm, the expression can be seen in Eq. (2), where the l_i represents the index of the peak p_i satisfying the condition. The used threshold parameters were validated similarly in a previous work (Boulos et al., 2011). As a different database was used in comparison to the previous study, different peak thresholds were varied and determined to be 25% for the given database.

Finally, the last stage of the eye movement detection algorithm ascertained the detected pulse edges for all the peaks found in the prior stage. Peaks were only acknowledged as proper movements if the peak returned to the baseline. Spikes in the signal could have been a result of incomplete eye movements or fluctuations, which would affect the baseline. Pulse edges were detected using samples before and after the time location of every qualified peak. Rising and falling edge refers to the detected edge of the peak that occurs immediately before and after the peak, respectively. For the i^{th} peak that was detected within the segment, the two edges must meet the required condition expressed in Eq. (3), where k corresponds to the index of time samples of the segmented signal. The $e(k)$ is then arranged in sequential order to identify the last/first found index that meets the required condition depending if the edge is rising or falling. The index was then stored accordingly as a rising edge RE_i or falling edge FE_i that corresponds to the peak p_i. To observe how each stage operates, the process is illustrated in Fig. 2. The peak threshold and pulse edge threshold are represented in red and black, respectively. The open pink circles represent the detected peaks, while the green line depicts the expected eye movements that were generated by the subject. After determining that the detected peaks were genuine eye movements, the next stage of verification was to determine if the movement was truly horizontal. As directionality and motion of the eyes are normally congruent, this phenomenon translates to an anti-phase difference between the left and right channel signals. The directionality of the movement was determined by confirming the peak amplitude and anti-phase relationship between the left and right channels. A version of the above detailed time-domain method for detecting eye movements was presented in our initial study (Liang et al., 2016).

2.3.1. Time domain features: rise-rate

In our previous analyses, we had tested the number of horizontal eye movements (i.e. count) in differentiating MG from controls (Liang et al., 2016). In the current analysis, we further studied the eye movement pulse characteristics and quantified them using the following time-domain features: Average Movement Count, Rise Rate, and Fall Rate. In the preliminary analyses of the evaluated

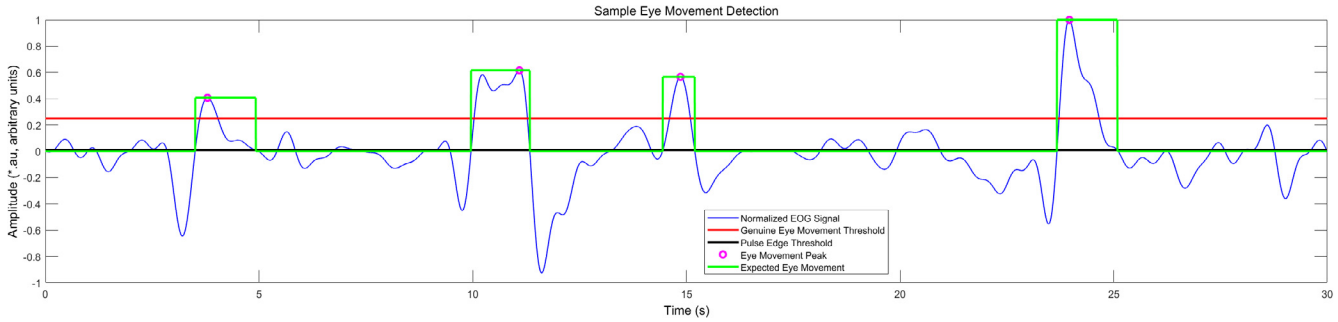

Fig. 2. Illustration of eye movement detection algorithm on a sample Electrooculography signal.

features, we found the distribution of the Rise Rate feature of the eye movement pulse to be discriminative in segregating MG from controls. To better represent the Rise Rate for any individual subject, the Rise Rate was calculated as described below for all segmented signals and then averaged. Empty segments or segments containing no movements as detected by the algorithm were removed.

The Rise Rate feature is defined as in Eq. (4). This feature is equivalent to a rate of change; hence, the Rise Rate feature can be considered as a first order derivative in the positive direction.

$$Rise\ \ Rate_i = \frac{p_i}{l_i - RE_i} \tag{4}$$

In Eq. (4), the p_i term represents the i^{th} peak's normalized amplitude and l_i term represents i^{th} peak index of segmented signal. The RE_i term represents the rising edge location. To better represent the Rise Rate for one subject, the Rise Rate was calculated for all segmented signals and then averaged.

2.4. Wavelet analysis: continuous wavelet transform (CWT)

Following the time-domain analysis described in the earlier section, we also performed wavelet analysis to capture EOG signal morphologies that could differentiate MG from control subjects. Wavelets are mathematical functions (or small waveforms) that incorporate specific properties and have definitive joint time and frequency localization. By changing the mother wavelet, different characteristics of the signal in the time-scale domain can be emphasized or captured. Depending on the nature of the application, proper wavelet selection can optimize the analyses.

The mother wavelet function is denoted as Ψ and is defined in Eq. (5) (Gao and Yan, 2011),

$$\Psi = \frac{1}{\sqrt{a}}\psi\left(\frac{t-b}{a}\right) \tag{5}$$

where a and b represent the scale parameter and translational parameter of the wavelet function, respectively. For a given signal $x(t)$ (EOG in our case) and mother wavelet function Ψ, the continuous wavelet transform (CWT) is expressed in Eq. (6) (Gao and Yan, 2011).

$$C_x(a,b) = \frac{1}{\sqrt{a}}\int_{-\infty}^{\infty} x(t)\psi^*\left(\frac{t-b}{a}\right)dt \tag{6}$$

Shown in Eq. (6), the mother wavelet function behaves as a window and the properties of the window are controlled by the a and b parameters. The scale parameter a has an inverse relation to frequency. Global information of the signal is represented in the high scale (or low frequency) values, and conversely localized or details of the signal are represented in the low scale (or high frequency) values (Rafiee et al., 2011). The parameter b controls the translation window in time. From our application point of view, in simple words, we are trying to find the best matching wavelet (or small waveform) that correlates well with EOG signal morphologies that differentiate MG from control subjects. After applying CWT, coefficients generated for each translation and scaling of the wavelet function are then used to form a matrix. Using the energy of each calculated wavelet coefficient, a scalogram can be computed. This scalogram depicts the local time-scale energy densities which is defined as $|C_x(a,b)|^2$. In the scalogram, the regions corresponding to a particular combination of translation (time) and scaling (inversely related to frequency) of a specific mother wavelet produces proportionate high energy accumulation depending upon its correlation or a match with signal morphologies within the EOG signals.

When applying the CWT, the scale range was limited to match the bandpass filter frequency range that was used. Despite the CWT expression being continuous, for the computer implementation, the following discretized form was used in Eq. (7) (Angrisani et al., 1998).

$$D_x(s,g) = \frac{1}{\sqrt{s}}\sum_{n=1}^{N} x[n]\psi^*\left(\frac{n-g}{s}\right) \tag{7}$$

In Eq. (7), the term s represents the scale, g represents the translation, and $D_x(s,g)$ represents the wavelet coefficients for the discrete time EOG signal $x[n]$.

2.4.1. Wavelet domain features: scale band energy (SBE)

In the wavelet analysis we explored the energy associated with scale bands, as the goal was to capture time and frequency range characteristics of the EOG morphologies that could be restricted to certain wavelet scales. One such feature, the scale band energy (SBE) as described below was found to perform best in segregating the groups.

For a given segment of the signal $x[n]$, normalization in energy is expressed in Eq. (8).

$$x_{norm}[n] = \frac{x[n]}{||x[n]||} \tag{8}$$

Once the normalization of energy was applied, identical subbands in the time-scale domain can be compared. Specific localized scale bands were targeted that may contain the morphology of interest for the detection of MG. Energy captured in a particular scale band is given by Eq. (9).

$$SBE_x = \sum_{g=1}^{l}\sum_{s=q_1}^{q_2}|D_x(s,g)|^2 \tag{9}$$

In Eq. (9), the $D_x(s,g)$ term is the wavelet coefficient at time sample or translation g, scale s, the term l represents the total number of columns or time samples, and the $q_1 : q_2$ represents the scale band. Scales corresponding to the higher frequencies of the signal were targeted to best represent the morphology of MG. To further optimize the analysis, different wavelet functions were applied and we searched for the optimal scale bands. The wavelet function that had the best performance with the SBE feature was the "Mexican Hat" type function (Mallat, 2008).

Using the Mexican Hat wavelet, the best performing scales corresponded to a frequency range of 0.8 to 1.42 Hz. After calculating the total scale band energy value for each signal segment, a median based averaging approach was applied. The wavelet approach was adaptive and, in contrast to time-domain features, no locations (i.e. eye movements or segments) were predetermined for the analysis. Nonetheless, instances where a segment may have had an abnormally low or high feature value were possible. Hence, the use of a median-based averaging approach was preferred, which was more resilient to the effects of potential outliers. The SBE feature was extracted from the left and right channels separately and averaged between the channels to form the Mean SBE feature.

A feature's ability to separate the two study groups was examined by using a Fisher's linear discriminant analysis (LDA) based classifier (Duda et al., 2012; IBM Corp. Released 2017). In addition, the leave-one-out cross validation (LOOCV) method permitted evaluation of a classifier's robustness (Duda et al., 2012; IBM Corp. Released 2017). For both the time-domain and wavelet approaches, the three different data sets used generated three different classification accuracies. Receiver operating characteristic (ROC) curves were used to provide an additional step of validation, computed with the use of R software (R Core Team, 2018).

3. Results

We report the time-domain approach results followed by, the wavelet approach results. Although few features and their statistical variants were explored, a stepwise feature selection method using IBM SPSS software package (IBM Corp. Released 2017) was used to identify the dominant features. In the stepwise feature selection process, the feature selection was performed in a cross-validated fashion i.e. feature selection was performed within each of the folds of the LOOCV and the number of times a feature was selected was computed. The most frequently chosen feature was then selected for further analysis. Boxplot figures were used to display the separation ability of the features visually, whereas the classification accuracies demonstrated the separation abilities quantitatively.

3.1. Time domain results

As explained earlier, although we tested 3 features, Average Movement, Rise Rate, and Fall Rate, the Rise Rate feature was dominant in segregating the groups better than any other combination of the 3 features. During the cross-validated stepwise feature selection process, the Rise Rate feature was chosen 97% of the time and the Fall Rate was chosen 3% of the time on an average over the 3 data sets. The mean and standard deviation of these features for Group All, MSLT, and PSG are as follows: Average Movement Count [MG – 161.63 ± 63.36, 159.50 ± 61.23, 163.75 ± 69.59 and Controls – 85.02 ± 58.14, 83.42 ± 53.42, 182.75 ± 52.01], Rise Rate [MG – 1.40E−3 ± 5.87E−4, 1.40E−3 ± 5.52E−4, 1.40E−3 ± 6.58E−4 and Controls – 5.77E−4 ± 5.17E−4, 5.50E−4 ± 5.00E−4, 1.99E−3 ± 5.52E−4], and Fall rate [MG – 1.20E−3 ± 4.99E−4, 1.20E−3 ± 4.82E−4, 1.20E−3 ± 5.49E−4 and Controls – 5.68E−4 ± 4.58E−4, 5.37E−4 ± 4.19E−4, 1.62E−3 ± 4.80E−4] respectively.

For all 3 data sets (Group All, Group MSLT, and Group PSG), the Rise Rate feature was also statistically significant in classifying MG from controls with P values of 8.754×10^{-7}, 0.0003, and 0.001133 respectively. The box plots in Fig. 3 illustrate the differences in the distribution of the Rise Rate feature for the MG and Control subjects. For the Group All, the LOOCV based classification accuracies were computed and are reported in the top portion of Table 1. The overall classification accuracy was found to be 83.3% with a sensitivity of 68.75% and a specificity of 87.1%. A weighted mean approach was used to compute the overall classification accuracy and hence the overall accuracy in this scenario was biased by the high specificity for the larger control group. The area under the ROC curve (AUC) was also computed, a technique that is particularly useful in situations where the data sets are imbalanced. The ROC curves for the 3 data sets are shown in Fig. 4. For the data set Group All, the AUC was found to be 0.88. For the Group MSLT data set, the LOOCV based classification accuracies were computed and reported in the middle portion of Table 1. An overall classification accuracy of 82.1% was found with a sensitivity of 62.5% and a specificity of 87.1%. The AUC was found to be 0.91. Similarly, using data set Group PSG, the LOOCV based classification accuracies are reported in the bottom portion of Table 1. An overall classification accuracy was found to be 82.1% with a sensitivity of 62.5% and a specificity of 87.1%. The AUC was found to be 0.87. Likewise, although Rise Rate was the dominant or most chosen feature, we have also provided the individual classification accuracies obtained for the 3 data sets using the Fall Rate and Average Movement Count features in Tables 2 and 3 respectively.

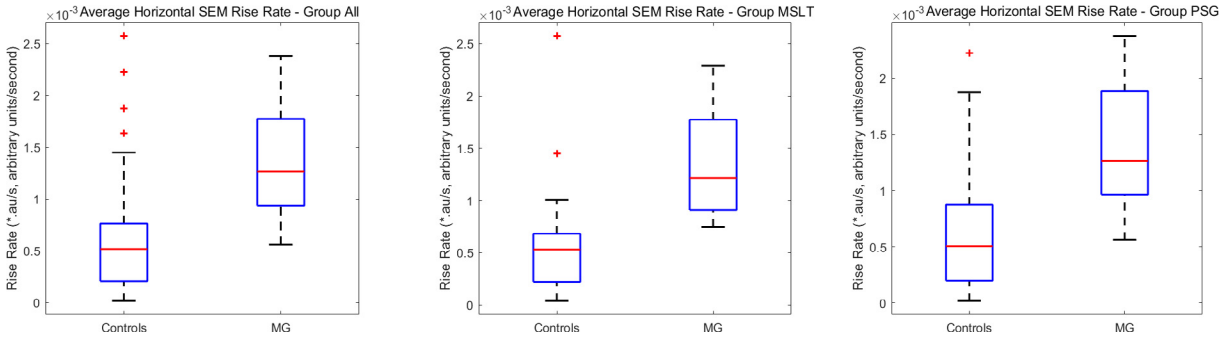

Fig. 3. Boxplots of Rise Rate feature for Group All, Group Multiple Sleep Latency Test (MSLT), and Group Polysomnography (PSG).

Table 1
Leave-one-out (LOO) cross validated classification accuracy using Rise Rate feature for Group ALL (top panel), Group Multiple Sleep Latency Test (MSLT) (middle panel), and Group Polysomnography (PSG) (bottom panel). MG – Myasthenia Gravis and NC – Normal Controls.

Method	Groups	MG	NC	Total
Group ALL				
Cross-Validated	MG	**11**	5	16
	NC	8	**54**	62
%	MG	**68.75**	31.25	100
	NC	12.9	**87.1**	100
Group MSLT				
Cross-Validated	MG	**5**	3	8
	NC	4	**27**	31
%	MG	**62.5**	37.5	100
	NC	12.9	**87.1**	100
Group PSG				
Cross-Validated	MG	**5**	3	8
	NC	4	**27**	31
%	MG	**62.5**	37.5	100
	NC	12.9	**87.1**	100

The numbers (and percentages) in bold fonts correspond to the correct classifications i.e. the number (and percentage) of samples that were correctly classified as their true state.

3.2. Wavelet domain results

The wavelet results were similarly quantified with the use of an LDA based classification and cross-validated using the LOOCV method. For all 3 data sets (Group All, Group MSLT, and Group PSG), the Mean SBE feature (using Mexican Hat Wavelet) was statistically significant in classifying MG from controls with P values of 2.024×10^{-7}, 0.00475, and 0.000077 respectively. The mean

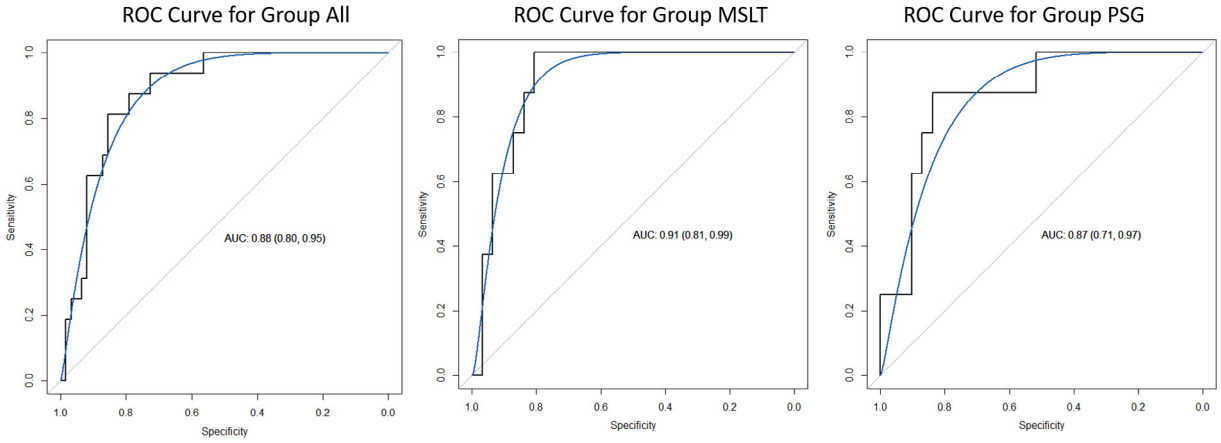

Fig. 4. Receiver Operating Characteristics (ROC) curves for the Rise Rate feature. Group ALL, Group Multiple Sleep Latency Test (MSLT), and Group Polysomnography (PSG).

Table 2
Leave-one-out (LOO) cross validated classification accuracy using Fall Rate feature for Group ALL (top panel), Group Multiple Sleep Latency Test (MSLT) (middle panel), and Group Polysomnography (PSG) (bottom panel). MG – Myasthenia Gravis and NC – Normal Controls.

Method	Groups	MG	NC	Total
Group ALL				
Cross-Validated	MG	**11**	5	16
	NC	11	**51**	62
%	MG	**68.75**	31.25	100
	NC	17.7	**82.3**	100
Group MSLT				
Cross-Validated	MG	**6**	2	8
	NC	4	**27**	31
%	MG	**75.0**	25.0	100
	NC	12.9	**87.1**	100
Group PSG				
Cross-Validated	MG	**6**	2	8
	NC	8	**23**	31
%	MG	**75.0**	25.0	100
	NC	25.8	**74.2**	100

The numbers (and percentages) in bold fonts correspond to the correct classifications i.e. the number (and percentage) of samples that were correctly classified as their true state.

Table 3
Leave-one-out (LOO) cross validated classification accuracy using Average Movement Count feature for Group ALL (top panel), Group Multiple Sleep Latency Test (MSLT) (middle panel), and Group Polysomnography (PSG) (bottom panel). MG – Myasthenia Gravis and NC – Normal Controls.

Method	Groups	MG	NC	Total
Group ALL				
Cross-Validated	MG	**10**	6	16
	NC	13	**49**	62
%	MG	**62.5**	37.5	100
	NC	21.0	**79.0**	100
Group MSLT				
Cross-Validated	MG	**5**	3	8
	NC	7	**24**	31
%	MG	**62.5**	37.5	100
	NC	22.6	**77.4**	100
Group PSG				
Cross-Validated	MG	**5**	3	8
	NC	7	**24**	31
%	MG	**62.5**	37.5	100
	NC	22.6	**77.4**	100

The numbers (and percentages) in bold fonts correspond to the correct classifications i.e. the number (and percentage) of samples that were correctly classified as their true state.

and standard deviation of the feature for Group All, MSLT, and PSG are as follows: [MG – 1399.80 ± 313.86, 1290.20 ± 325.77, 1509.40 ± 278.42 and Controls – 723.60 ± 444.37, 623.52 ± 460.96, 823.68 ± 410.27]. The box plots in Fig. 5 illustrate the difference in the distribution of the Mean SBE feature for the MG and Control subjects. The classification performance for data set Group All was computed and reported in the top portion of Table 4. An overall classification accuracy of 82.1% with a sensitivity of 87.5% and specificity of 80.6% was achieved. Unlike the time-domain feature, the results obtained for the wavelet approach yielded a more balanced sensitivity and specificity. The ROC curves for the 3 data sets are shown in Fig. 6. The AUC for Group All was found to be 0.89. For the Group MSLT data set, the classification performance was computed and tabulated in the middle portion of Table 4. The overall classification accuracy was found to be 87.2% with a sensitivity of 87.5% and a specificity of 87.1%. The AUC was found to be 0.89. Lastly, for the Group PSG data set, the classification performance was computed and tabulated in the bot-

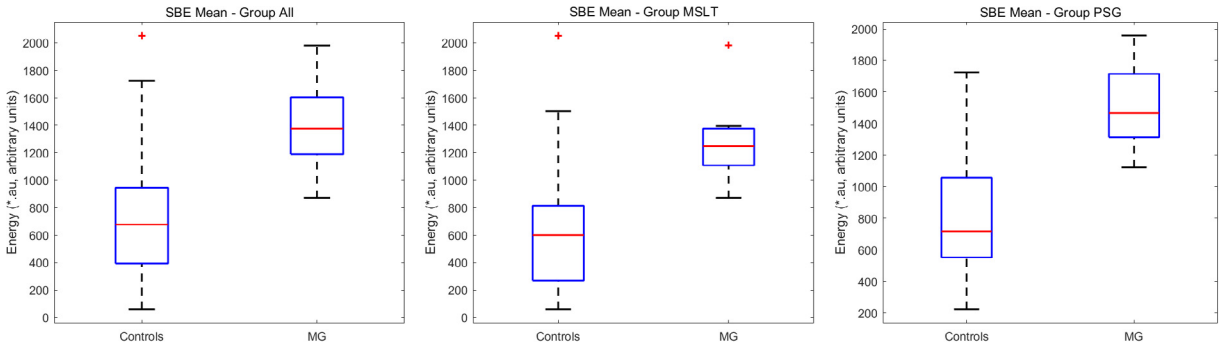

Fig. 5. Boxplots of Wavelet (Mexican Hat) Mean Scale Band Energy (SBE) feature for Group All, Group Multiple Sleep Latency Test (MSLT), and Group Polysomnography (PSG).

Table 4
Leave-one-out (LOO) cross validated classification accuracy using Wavelet (Mexican Hat) Mean Scale Band Energy (SBE) feature for Group ALL (top panel), Group Multiple Sleep Latency Test (MSLT) (middle panel), and Group Polysomnography (PSG) (bottom panel). MG- Myasthenia Gravis and NC – Normal Controls.

Method	Groups	MG	NC	Total
Group ALL				
Cross-Validated	MG	**14**	2	16
	NC	12	**50**	62
%	MG	**87.5**	12.5	100
	NC	19.4	**80.6**	100
Group MSLT				
Cross-Validated	MG	**7**	1	8
	NC	4	**27**	31
%	MG	**87.5**	12.5	100
	NC	12.9	**87.1**	100
Group PSG				
Cross-Validated	MG	**7**	1	8
	NC	6	**25**	31
%	MG	**87.5**	12.5	100
	NC	19.4	**80.6**	100

The numbers (and percentages) in bold fonts correspond to the correct classifications i.e. the number (and percentage) of samples that were correctly classified as their true state.

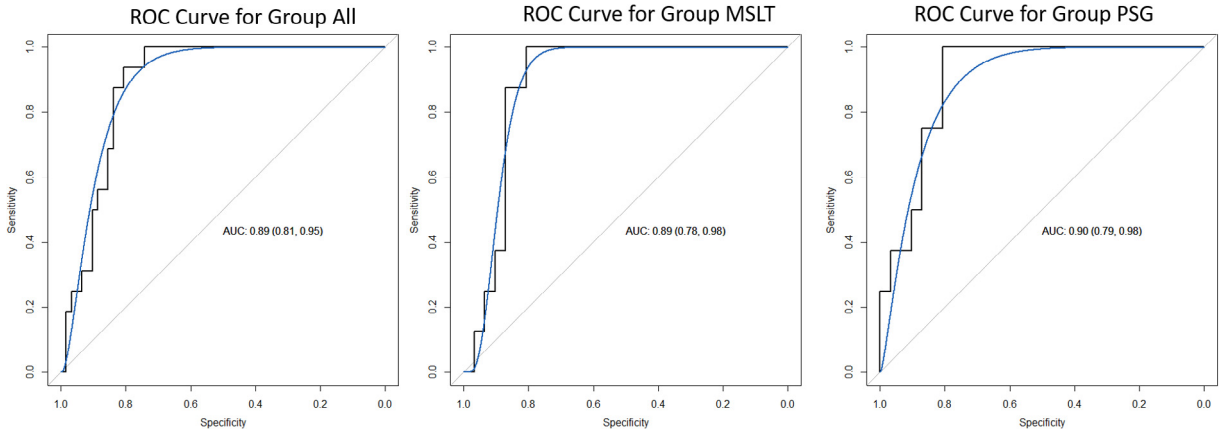

Fig. 6. Receiver Operating Characteristics (ROC) curves for the Wavelet (Mexican Hat) Mean Scale Band Energy (SBE) feature. Group ALL, Group Multiple Sleep Latency Test (MSLT), and Group Polysomnography (PSG).

tom portion of Table 4. The overall classification accuracy for Group PSG was found to be 82.1% with a sensitivity of 87.5% and a specificity of 80.6%. The AUC was found to be 0.90. The Mean SBE feature for all three data sets demonstrated to have a high level of robustness according to the AUC values found.

4. Discussion

This study presents a non-invasive method for detecting ocular motor dysfunction from MG using EOG signals, and we report three unique findings: First, our study showed that a simple Rise Rate feature extracted from time-domain analysis of EOG signals was effective in detecting MG, although there was a trade-off with sensitivity and specificity. Secondly, through the wavelet approach of using scale energy sub-banding, the morphology traits of MG that were different from the control group were approximately localized between frequencies of 0.8–1.42 Hz. Third, of all the examined wavelet functions, the Mexican Hat wavelet had the highest correlations with signal structures that may prove best to discriminate MG from controls.

Although classifications were performed with the other features (e.g. Average Movement Count and Fall Rate), the stepwise feature selection process identified the Rise Rate as the most chosen time-domain feature in all 3 data sets. We also tested the combination of these features but none of the combinations performed better than Rise Rate alone. The use of a single time domain feature (Rise Rate) successfully demonstrated that classifying MG from control data, regardless of the sleep test used, was possible during the wake stage. To be able to classify MG without the need for a specific sleep test indicates that EOG signals may inherently capture unique traits that belong to MG. From the boxplots for the Rise Rate feature, we observed that the distributions of the rise rate for the MG patients were greater than was seen in the control group. One possible explanation could be that the presence of involuntary/voluntary eye movements were greater in MG. These eye movements are potentially characterized by muscular twitching (i.e. eye movements that could reach their maximum velocities very quickly). The three data sets using time-domain approach resulted in overall accuracies of >80%, which illustrates that the use of EOG signals for this application is possible. However, the sensitivities and specificities were imbalanced. If the final objective was for early detection of MG, then obtaining balanced sensitivities and specificities would be more desirable.

Although time domain approaches demonstrated their viability, this approach was limited by a few factors. The results were heavily dependent on the normalization and segmentation processes. Normalization is a common procedure, however, the amplitude normalization used in this work is dependent on the signal being free of sudden or random spikes that were not generated by the subject. Using the segmentation process in conjunction reduces the negative effect of these sudden large pulses from the signal as it limits the artifact to a certain segment. By fixing the time length of the segment, the same eye movement could be counted twice depending on where the segmentation was taken. If a larger time segment was used instead, the likelihood of repeated or misinterpreted movements would decrease. However, it would increase the effects of potential irregular spikes. Thus, there is a trade-off for the selected size of the segmentation window.

The wavelet approach demonstrated that a single time-scale domain feature (i.e. Mean SBE) using the Mexican Hat wavelet function could successfully discriminate MG patients from the controls. The wavelet approach also produced more balanced sensitivities and specificities. Classification accuracies obtained using the wavelet approach suggested there could be the potential for MG detection as well as screening using this approach. By observing the boxplots for the Mean SBE feature, the MG group demonstrated a higher Mean SBE value in comparison to the controls. The limited scale band of interest (0.8–1.42 Hz) with the Mexican Hat wavelet signal structure may hold a discriminatory EOG morphological clue in segregating MG from controls. Due to the adaptive nature of the wavelet approach, the requirement for selective threshold parameters was not required (but, conversely, was needed with the time-domain approaches). Based on the results obtained, the wavelet approach demonstrated better overall balanced performance in comparison to the time domain for the same database. Our findings demonstrated that regardless of the sleep test used, up to 10 min could be sufficient to achieve acceptable diagnostic accuracy and specificity, mitigating the need for overnight polysomnography in this group of patients. As there was no added benefit in using specific sleep tests for MG detection, no additional set-up other than 2 extra-ocular and 2 reference electrodes would be necessary to replicate this scenario in a clinic as long as a quiet recording environment allowing for 10 min of rest was provided.

Future work will focus on the sub-classification of MG from other non-MG ocular disorders, EOG morphology characterization in MG patients, and the potential development of practical tools that can facilitate the early detection/screening of MG in clinics. In addition, the minimal EOG recording time duration required to achieve accurate results will also be objectively validated.

Acknowledgements

The authors thankfully acknowledge Ryerson University and Natural Sciences and Engineering Research Council of Canada (Grant No: RGPIN-2015-06644) for funding this work.

Declaration of Competing Interest

None of the authors have potential conflicts of interest to be disclosed.

References

Angrisani L, Daponte P, D'Apuzzo M, Testa A. A measurement method based on the wavelet transform for power quality analysis. IEEE Trans Power Deliv 1998;13:990–8.

Azri M, Young S, Lin H, Tan C, Yang Z. Diagnosis of Ocular Myasthenia Gravis by means of tracking eye parameters. In: 2014 36th annual international conference of the IEEE engineering in medicine and biology society; 2014. p. 1460–4.

Barton JJS. Quantitative ocular tests for myasthenia gravis: a comparative review with detection theory analysis. J Neurol Sci 1998;155:104–14.

Boulos MI, Umapathy K, Shokrollahi P, McConville KMV, Sudenis T, Jewell DR, et al. Automated detection of nocturnal slow eye movements modulated by selective serotonin reuptake inhibitors. Prog Neuropsychopharmacol Biol Psych 2011;35:126–30.

Duda RO, Hart PE, Stork DG. Pattern classification. John Wiley & Sons; 2012.

Gao RX, Yan R. Wavelets: theory and applications for manufacturing. US: Springer; 2011.

Gilhus NE. Autoimmune myasthenia gravis. Expert Rev Neurother 2009;9:351–8.

Iber C, Ancoli-Israel S, Chesson A, Quan SF. The AASM manual for the scoring of sleep and associated events: Rules, terminology and technical specifications. Vol. 1. Westchester, IL: American Academy of Sleep Medicine; 2007.

IBM Corp. Released 2017. IBM SPSS Statistics for Windows, Version 25.0. Armonk, NY: IBM Corp.

Kassardjian CD, Kokokyi S, Barnett C, Jewell D, Bril V, Murray BJ, et al. Excessive daytime sleepiness in patients with Myasthenia Gravis. J Neuromuscul Dis 2015;2:93–7.

Kupersmith MJ. Ocular myasthenia gravis: treatment successes and failures in patients with long-term follow-up. J Neurol 2009;256:1314–20.

Kushida CA, Littner MR, Morgenthaler T, Alessi CA, Bailey D, Coleman J, et al. Practice parameters for the indications for polysomnography and related procedures: an update for 2005. Sleep 2005;28:499–523.

Liang T, Boulos MI, Murray BJ, Krishnan S, Katzberg H, Umapathy K. Detection of myasthenia gravis using electrooculography signals. In: 2016 38th annual international conference of the IEEE engineering in medicine and biology society (EMBC); 2016. p. 896–9.

Littner MR, Kushida C, Wise M, Davila DG, Morgenthaler T, Lee-Chiong T, et al. Practice parameters for clinical use of the multiple sleep latency test and the maintenance of wakefulness test. Sleep 2005;28:113–21.

Magosso E, Ursino M, Provini F, Montagna P. Wavelet analysis of electroencephalographic and electro-oculographic changes during the sleep onset period. In: 2007 29th annual international conference of the IEEE engineering in medicine and biology society; 2007. p. 4006–10.

Mallat S. A wavelet tour of signal processing: the sparse way. Academic Press; 2008.

Martínez-Lapiscina EH, Martínez De Lapiscina EH, Erro ME, Erro Aguirre ME, Ayuso T, Ayuso Blanco T, et al. Myasthenia gravis: sleep quality, quality of life, and disease severity. Muscle Nerve 2012;46:174–80.

Mee J, Paine M, Byrne E, King J, Reardon K, O'day J. Immunotherapy of ocular myasthenia gravis reduces conversion to generalized myasthenia gravis. J Neuroophthalmol 2003;23:251–5.

Nair AG, Patil-Chhablani P, Venkatramani DV, Gandhi RA. Ocular myasthenia gravis: a review. Indian J Ophthalmol 2014;62:985–91.

R Core Team. R: A language and environment for statistical computing. R Found Stat Comput Vienna Austria; 2018. Available from: https://www.R-project.org/.

Rafiee J, Rafiee MA, Prause N, Schoen MP. Wavelet basis functions in biomedical signal processing. Expert Syst Appl 2011;38:6190–201.

Sonett JR, Magee MJ, Gorenstein L. Thymectomy and myasthenia gravis: a history of surgical passion and scientific excellence. J Thorac Cardiovasc Surg 2017;154:306–9.

Valko Y, Rosengren SM, Jung HH, Straumann D, Landau K, Weber KP. Ocular vestibular evoked myogenic potentials as a test for myasthenia gravis. Neurology 2016;86:660–8.